Results of corrosion tests in liquid Pb-Bi at JAEA – temperature and oxygen concentration dependence, and corrosion properties of Si-enriched steels

Yuji Kurata, Shigeru Saito
Japan Atomic Energy Agency, Japan

Abstract

Corrosion tests of various steels in liquid Pb-Bi have been conducted using static corrosion apparatus. Effects of temperature, oxygen concentration in liquid Pb-Bi and alloying elements in steels on corrosion behaviour have been estimated. Temperature ranges of the corrosion tests were from 450°C to 600°C. Corrosion tests were conducted under the oxygen-saturated condition and the low oxygen concentration condition. Effects of alloying elements such as Cr, Ni and Si have been investigated. Furthermore, corrosion properties of Si-enriched Mod.9Cr-1Mo steel and Si-enriched 316SS are presented.

Introduction

Lead-bismuth eutectic (LBE) is a promising candidate material of core coolants and high-power spallation targets of accelerator driven systems (ADS) for transmutation of radioactive wastes and of coolants of fast reactors (FR). However, compatibility of materials with liquid LBE is one of critical issues to develop the ADS and the FR.

The study on the compatibility of materials with liquid LBE has been conducted in Russia since the early stage of nuclear reactor development and fruitful results have been obtained [1,2]. It was shown that the 12%Cr martensitic steel with Si addition developed in the Russian study exhibited good corrosion resistance in liquid LBE [2-4]. The extensive results of LBE corrosion study, which has received significant attention and been performed worldwide recently, are compiled in an OECD/NEA handbook [5]. Although many corrosion data in LBE have been reported, the reliable data are not still enough to predict corrosion properties of steels quantitatively under various conditions. Effects of temperature [4,6] and oxygen concentration [6] on corrosion properties of steels in LBE were also reported. However, it is necessary to get data of experiments conducted systematically for various steels because the results obtained are still scarce and scattered. It was reported that the 12%Cr martensitic steel containing 1.8% Si [2] and the austenitic stainless steel containing about 5% Si [7] showed good corrosion resistance in liquid LBE. On the other hand, it is essential that steels used for nuclear reactors have also good radiation resistance. 316SS and T91 (Mod.9Cr-1Mo steel) are favourable due to their abundant irradiation data and their good radiation resistance from the viewpoint of irradiation performance. Therefore, the improvement of corrosion resistance of 316SS and T91 by the addition of Si is one of methods to develop materials used in LBE.

In the present paper, effects of temperature and oxygen concentration on corrosion behaviour are made clear through static corrosion tests of various steels in liquid LBE. Furthermore, corrosion properties of Si-enriched T91 and Si-enriched 316SS are investigated.

Experimental

Materials and specimens

Table 1 shows chemical compositions of materials used in the experiment. F82H, T91, 410SS, 2.25Cr-1Mo steel, pure iron and Si-T91 are ferritic/martensitic steels. JPCA (14Cr-16Ni-2Mo), 316SS, SX, ZeCor and Si-316SS are austenitic stainless steels. SX and ZeCor are steels developed for use in a sulphuric acid environment and the characteristic of the steels is high Si content of about 5%. Si-T91 contains about 1.5% Si and Si-316SS contains about 2.5% Si. Corrosion specimens are rectangular plates with the size of 15 mm × 30 mm × 2 mm, and a hole of 7.2 mm diameter is made for installation at the upper part of the specimen. The surface of corrosion specimens is polished using emery papers up to #600.

Table 1: Chemical compositions of materials tested in the corrosion experiment (wt.%)

	C	Si	Mn	Cr	Ni	Mo	Fe	V	W	Cu
F82H[*1]	0.095	0.10	0.01	7.72	<0.02	<0.01	Bal.	0.18	1.95	–
T91 (Mod.9Cr-1Mo steel)[*1]	0.10	0.30	0.40	8.41	0.06	0.88	Bal.	0.20	<0.0005	–
JPCA (14Cr-16Ni-2Mo)[*2]	0.058	0.50	1.54	14.14	15.87	2.29	Bal.	0.03	0.010	–
410SS[*1]	0.067	0.31	0.80	12.21	0.12	0.02	Bal.	0.07	–	–
2.25Cr-1Mo steel[*1]	0.10	0.34	0.44	2.18	0.02	0.92	Bal.	0.01	–	–
Pure iron[*1]	0.002	–	–	–	–	–	Bal.	–	–	–
316SS[*2]	0.04	0.69	1.22	16.83	10.79	2.06	Bal.	–	–	–
SX[*2, *3]	0.010	4.80	0.60	17.58	19.08	0.356	Bal.	–	–	2.14
ZeCor[*2, *4]	0.014	5.76	0.59	13.59	15.72	1.02	Bal.	–	–	1.04
Si-T91[*1]	0.130	1.45	0.52	8.10	0.99	0.86	Bal.	0.20	–	–
Si-316SS[*2]	0.080	2.43	0.11	15.95	15.09	2.07	Bal.	<0.01	–	–

[*1] Ferritic/martensitic steels.

[*2] Austenitic steels.

[*3] Trademark of the Sandvik Corporation.

[*4] Trademark of Allegheny Ludlum Company.

Corrosion test apparatus and procedure

The static corrosion test apparatus in liquid LBE was described in detail elsewhere [8]. Components contacting liquid LBE were made of quartz. As received eutectic Pb-Bi (45Pb-55Bi) of 7 kg was used in each test of the present experiment. The LBE was melted in Ar cover gas with purity of 99.9999%.

The following three series of tests were conducted in this study: *i)* test to investigate temperature effect (Test-1); *ii)* test to investigate oxygen concentration effect (Test-2); *iii)* test to study effect of Si addition to T91 and 316SS (Test-3). Corrosion tests were done in oxygen-saturated LBE at 450°C, 500°C, 550°C and 600°C in Test-1. The corrosion test time was 3 000 h at 450°C and 550°C, and it was 2 000 h at 500°C and 600°C. Oxygen concentration under the saturated condition was 3×10^{-4} wt.% at 450°C, 6×10^{-4} wt.% at 500°C, 1×10^{-3} wt.% at 550°C and 2×10^{-3} wt.% at 600°C. In Test-2, corrosion tests under low oxygen concentration conditions were conducted at 450°C and 550°C for 3 000 h and the results were compared with those in Test-1 under the oxygen-saturated condition. Ar-4%H_2 gas was bubbled in the liquid LBE to produce low oxygen concentration conditions. The oxygen concentration was measured using an oxygen sensor of ZrO_2-8mol%Y_2O_3 with a reference electrode of Pt/air system. Oxygen concentrations in liquid LBE bubbled by Ar-4%H_2 gas were estimated to be 5×10^{-8} wt.% at 450°C and 3×10^{-9} wt% at 550°C, respectively. In Test-3, corrosion tests of Si-T91, Si-316SS and comparative materials were done in oxygen-saturated LBE at 450°C and 550°C for 3 000 h. The conditions of oxygen concentrations and temperatures in the present study are indicated as circles in Figure 1.

**Figure 1: Oxygen potential diagram and experimental conditions**
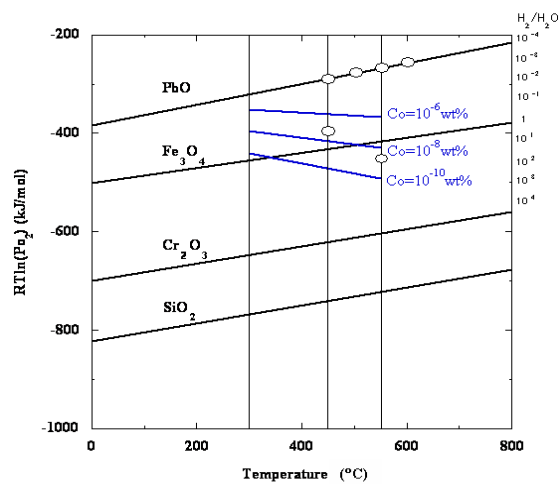
Test specimens were rinsed in silicone oil or glycerin after the corrosion tests to remove adherent LBE. The cut specimens were plated with copper and moulded into resin to protect corrosion films during polishing. Analyses were made using an optical microscope, a scanning electron microscope (SEM) with energy dispersion X-ray (EDX) equipment and a laser microscope.

Results and discussion

Temperature dependence

Experimental results at 450°C and 550°C have been reported in Ref. [7]. Temperature dependence of corrosion in liquid LBE is investigated in the present study using test results at 500°C and 600°C together with those at 450°C and 550°C.

Figure 2 shows corrosion depths of various steels at 450°C and 500°C. The line of the corrosion depth, which is calculated for 3 000 h or 2 000 h from the corrosion depth of 100 µm per 600 days assuming a linear rule, is indicated as a tentative guideline in this figure. Main corrosion phenomenon is oxide film formation at 450°C and grain boundary corrosion/internal oxidation is a little recognised in 2.25Cr-1Mo steel and F82H. Corrosion depths of all steels are below the line of the corrosion depth

Figure 2: Corrosion depths of steels at 450°C and 500°C
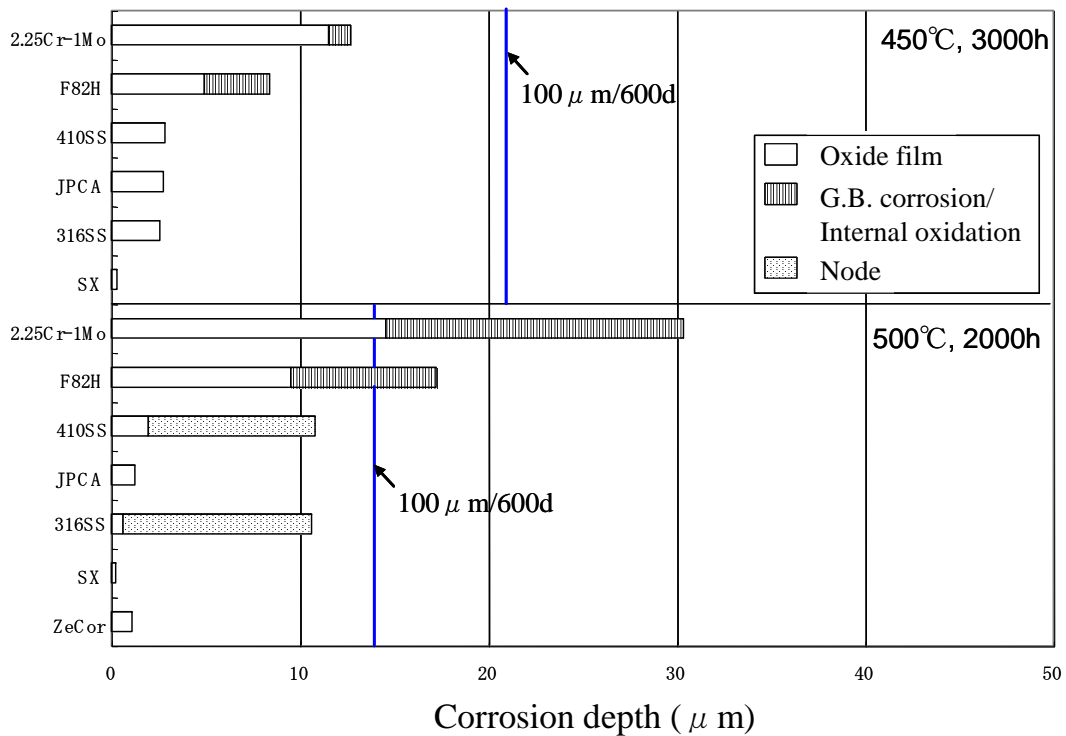
Corrosion depth (μ m)

of 100 μm per 600 days. The depth of grain boundary corrosion/internal oxidation becomes large at 500°C and oxide nodes appear in addition to oxide films on 410SS and 316SS. Figure 3 depicts optical micrographs of cross-sections of specimens after the corrosion test at 450°C. The corrosion film thickness changes depending on chemical compositions of various steels.
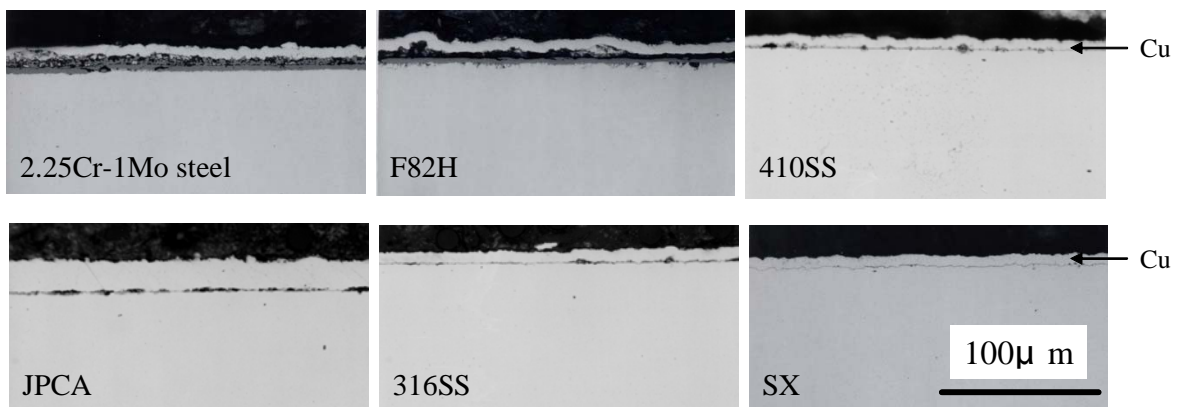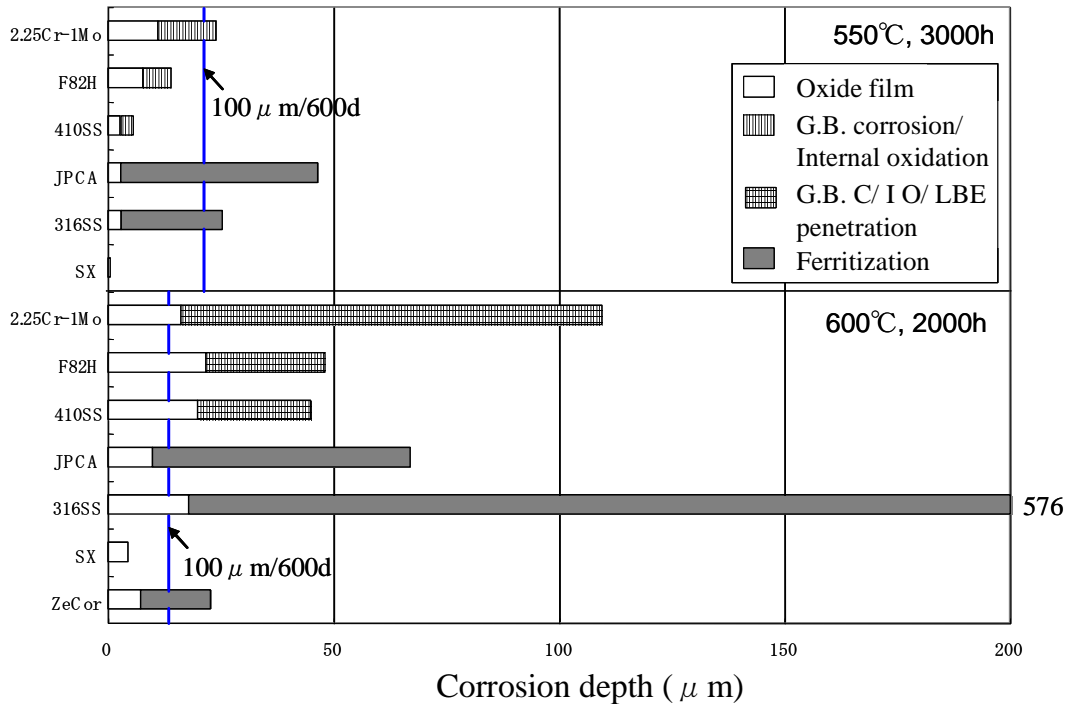
Figure 3: Optical micrographs of specimens after the corrosion test at 450°C

Figure 4 shows corrosion depths of various steels at 550°C and 600°C. The grain boundary corrosion/internal oxidation becomes significant in feritic/martensitic steels. Furthermore, ferritisation where Ni in steels dissolves into liquid LBE occurs for austenitic stainless steels such as JPCA and 316SS at 550°C. Figure 5 depicts optical micrographs of cross-sections of specimens after the corrosion test at 550°C. The above-mentioned characteristic of corrosion at 550°C is expressed in this figure. Ferritisation is not observed for SX containing about 5% Si in the corrosion test under the oxygen-saturated condition at 550°C for 3000 h.

Figure 4: Corrosion depths of steels at 550°C and 600°C

As indicated in Figure 4, severe corrosion occurs at 600°C. The LBE penetration goes together with the grain boundary corrosion/internal oxidation at 600°C. In addition, ferritisation is significant and, in particular, the corrosion depth of 316SS is above 500 μm for 2 000 h. When SX and ZeCor are compared, the corrosion depth of SX is smaller than that of ZeCor. The corrosion depths of steels except SX are larger than the line of the corrosion depth of 100 μm per 600 days. Figure 6 depicts optical micrographs of cross-sections of specimens after the corrosion test at 600°C. The above-mentioned characteristic of corrosion at 600°C is also expressed in this figure. Thinning occurs in 2.25Cr-1Mo steel and 316SS since grains drop out on account of severe internal oxidation, ferritisation and LBE penetration. Local ferritisation is observed in ZeCor in addition to the area where ferritisation is prevented. Examples of severe corrosion at 600°C are shown in Figure 7. Grain boundary corrosion/ internal oxidation and hollows are observed with LBE penetration in F82H. Significant thinning is recognised in 316SS together with ferritisation and LBE penetration.
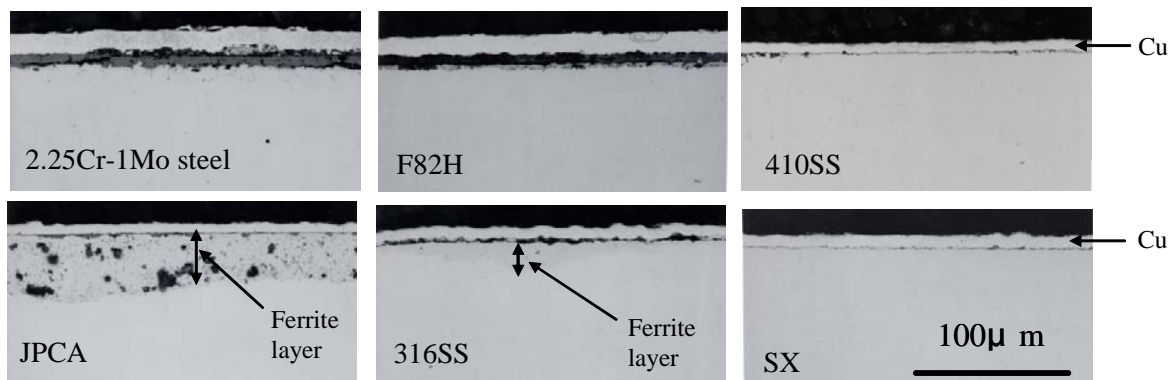
Figure 5: Optical micrographs of specimens after the corrosion test at 550°C

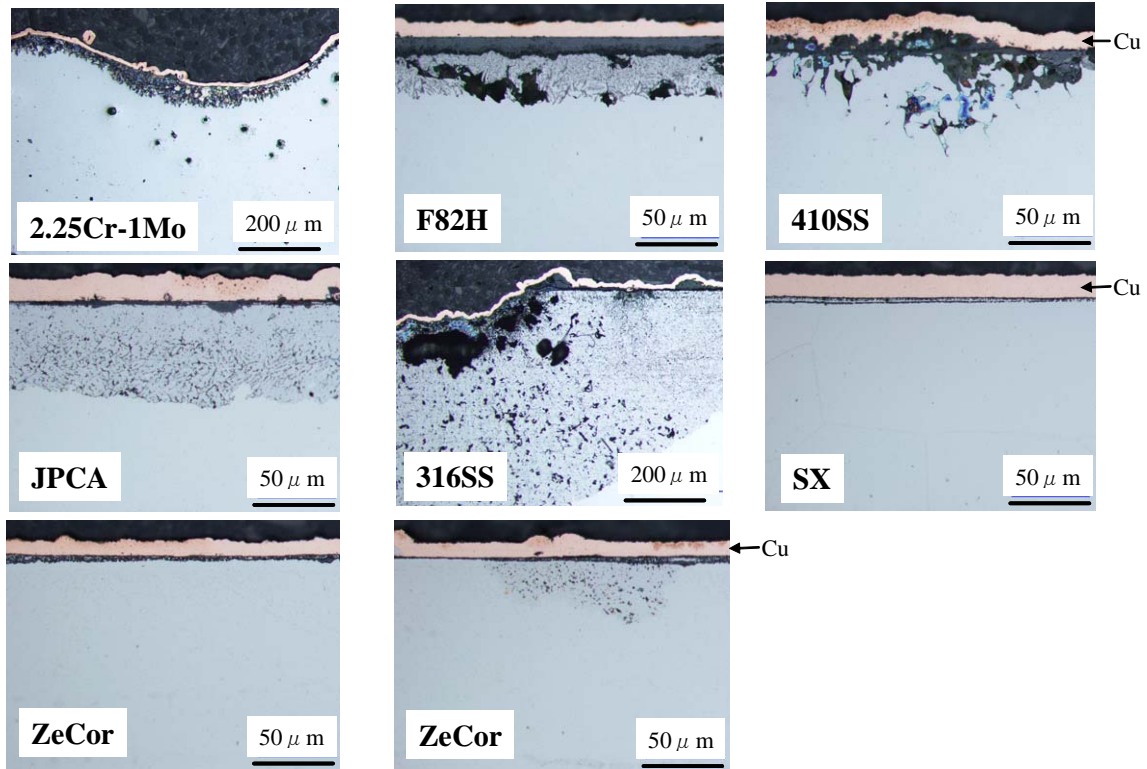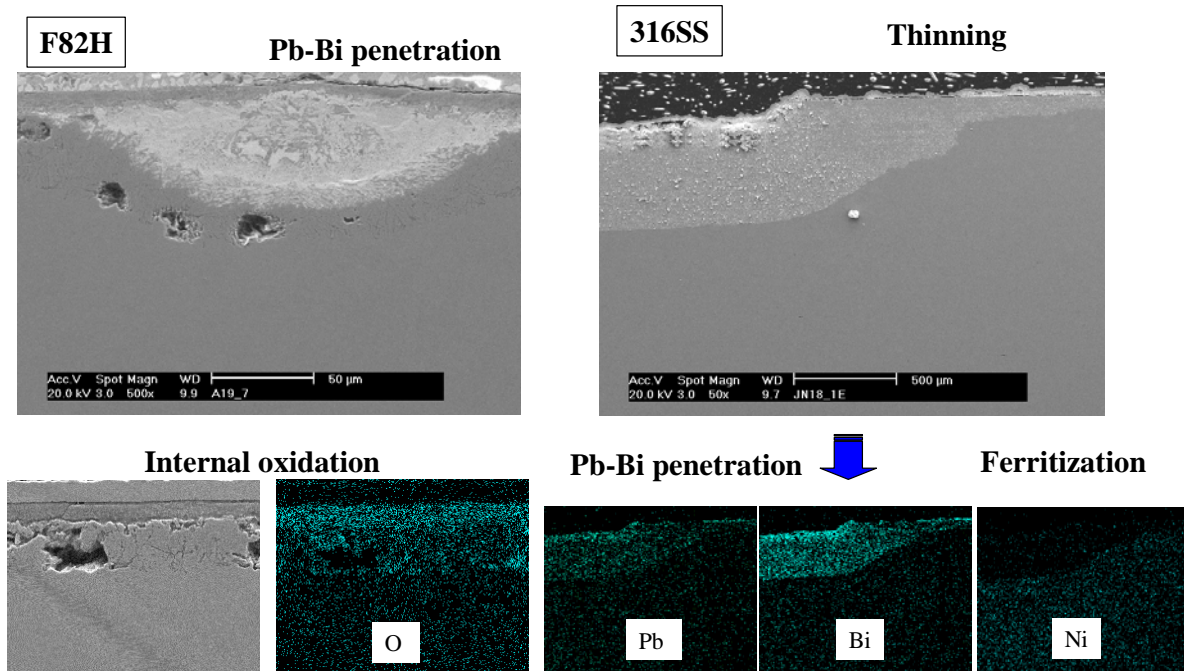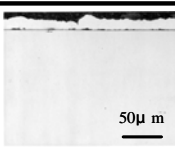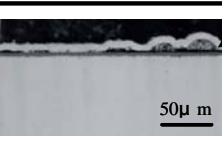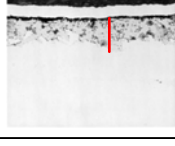**Figure 6: Optical micrographs of specimens after the corrosion test at 600°C**
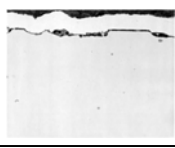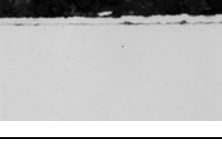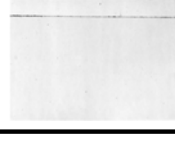

Figure 7: Characteristic of corrosion in LBE at 600°C

Oxygen concentration dependence

Experimental results under the condition of low oxygen concentration have been reported in Ref. [8]. Experimental results at 450°C and 550°C under the condition of low oxygen concentration are compared with those under the oxygen-saturated condition. Figure 8 shows effect of oxygen concentration on corrosion behaviour in LBE at 450°C. There is little influence on corrosion behaviour of T91 and SX at 450°C when the oxygen concentration in LBE decreases from 3×10^{-4} wt.% to 5×10^{-8} wt.%. Only oxide film thickness decreases in T91 under the low oxygen concentration condition. However, dissolution of Fe atoms occurs from the surface of the pure iron specimen under the low oxygen concentration condition at 450°C in spite of formation of very thin Fe-oxide film. As a result, the rough surface is formed on pure iron specimen. Ferritisation and penetration of LBE occur in 316SS under the low oxygen concentration condition at 450°C.

Figure 8: Effect of oxygen concentration in LBE on corrosion behaviour at 450°C

As shown in Figure 9, the influence of oxygen concentration decrease on corrosion behaviour becomes severe at 550°C. The corrosion type of T91 changes from simple oxidation to grain boundary corrosion, dissolution of elements and penetration of LBE at 550°C when the oxygen concentration in LBE decreases from 1×10^{-3} wt.% to 3×10^{-9} wt%. Severe dissolution proceeds in pure iron without oxide film formation under the low oxygen concentration condition at 550°C. The depth of ferritisation and LBE penetration is very large in 316SS under the low oxygen concentration condition at 550°C compared with that under the oxygen-saturated condition. Local ferritisation occurs under the low oxygen concentration condition at 550°C in SX which exhibits good corrosion resistance under the oxygen-saturated condition. Figure 10 shows three-dimensional images taken by a laser microscope for the surface of pure iron specimens after the corrosion tests. It is found that Fe atoms dissolve at both temperatures in liquid LBE with low oxygen concentrations. Dissolution of Fe atoms occurs initially at grain boundaries and proceeds to deep levels under the low oxygen concentration condition at 550°C.

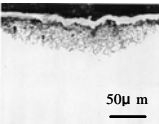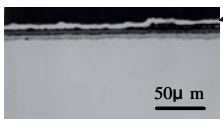**Figure 9: Effect of oxygen concentration in LBE on corrosion behaviour at 550°C**

Sample	Oxygen concentration 3x10⁻⁹%		Oxygen concentration 1x10⁻³%		Remarks

Oxygen concentration — 3x10⁻⁹% ← **Decrease** — 1x10⁻³%
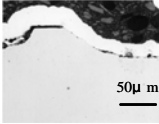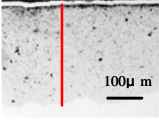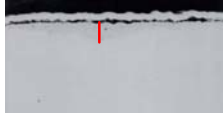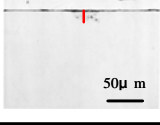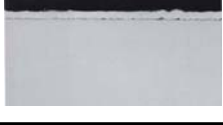
Sample	3x10⁻⁹%		1x10⁻³%		Remarks
T91		Thin oxide film, GB corrosion		Oxidation (Cu)	GB corrosion, Dissolution, LBE penetration
Pure iron		No oxide film, Dissolution		Oxidation	Severe dissolution occurs.
316 SS		Ni, Cr Dissolution, LBE penetration		Oxidation, Ferritization	Severe ferritization occurs.
SX (5%Si)		Local attack, LBE penetration		Oxidation	Local ferritization occurs.

Figure 10: Three-dimensional images of surfaces of pure iron specimens after corrosion tests in low oxygen concentration LBE at (a) 450°C and (b) 550°C
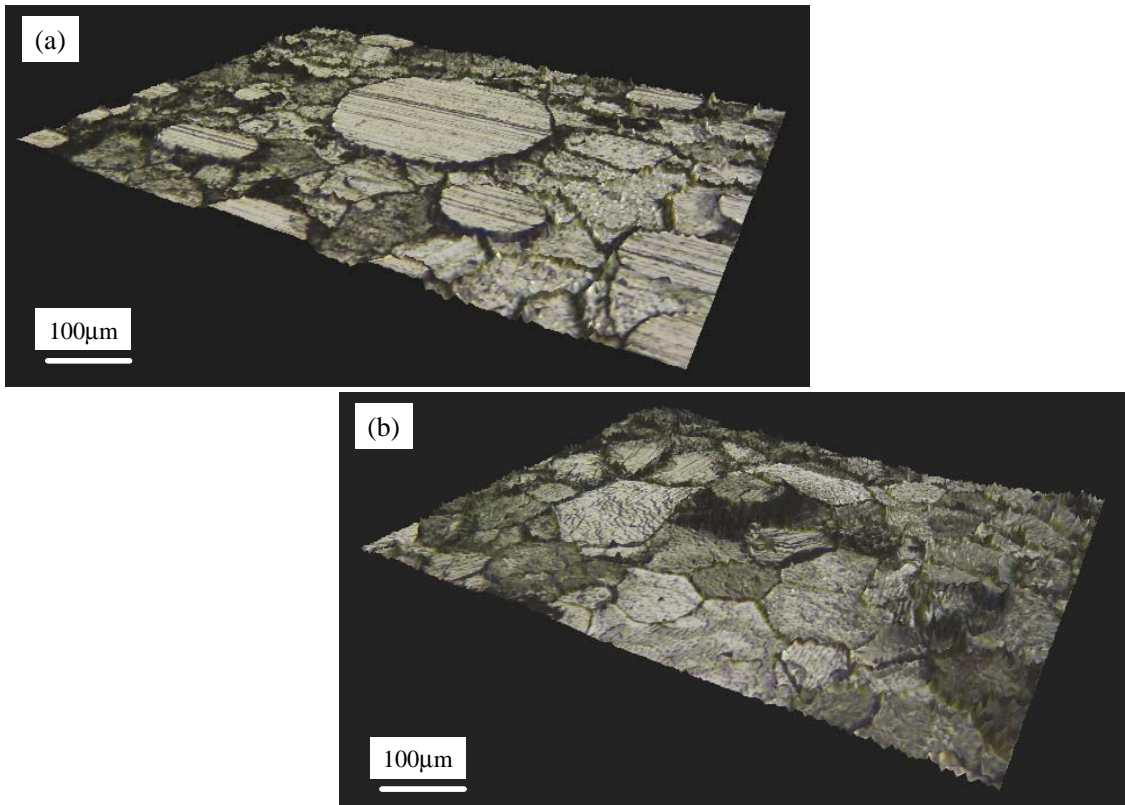
Corrosion properties of Si-enriched steels

Corrosion tests of Si-T91 and Si-316SS were conducted together with comparative materials in oxygen-saturated LBE at 450°C and 550°C for 3 000 h. Results of the corrosion test at 550°C where severe corrosion effects are produced are described in the present paper. Figure 11 depicts optical micrographs of cross-sections of specimens after the corrosion test at 550°C. Oxide film formation and grain boundary corrosion are observed in T91 and the corrosion depth attains 30 µm. A uniform oxide film is formed in Si-T91 and grain boundary corrosion is mitigated. As a result, the corrosion depth of Si-T91 is about 10 µm. While the depth of ferritisation of 316SS attains about 100 µm, only local ferritisation is observed in Si-316SS. This type of local ferritisation is also recognised in ZeCor containing about 5 wt.% Si. From these results it may be difficult to prevent the ferritisation of austenitic stainless steels completely by means of only addition of Si up to about 5 wt.%.

Figure 11: Effect of Si addition on corrosion behaviour of T91 and 316SS
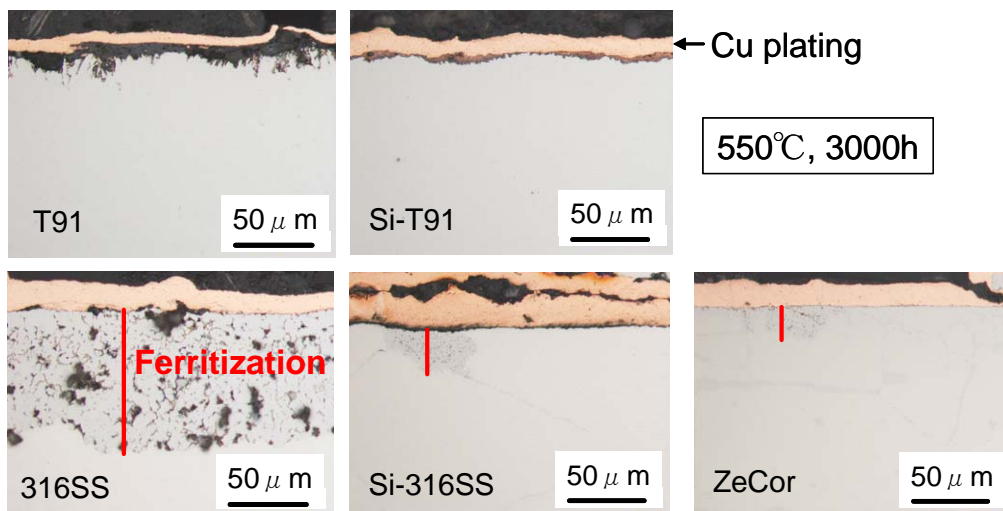
Figure 12 shows the result of line analyses of the cross-sections of Si-T91 and Si-316SS after the corrosion test in LBE at 550°C for 3 000 h. The corrosion film formed on the surface of Si-T91 is an oxide film containing Cr, Si and Fe. In this way, a Si-rich oxide film is formed on Si-T91 which contains about 1.5 wt.% Si. The Si-rich oxide film produces better corrosion resistance in comparison with Cr-Fe oxide formed on normal T91 where Si content is small. As indicated in Figure 12, Cr and Si are enriched in an oxide film formed on Si-316SS. However, dissolution of Ni and penetration of LBE are observed under the oxide film of Si-316SS. It is anticipated that the oxide film formed on Si-316SS does not have sufficient protectiveness because ferritisation occurs at some places.

Figure 12: Line analyses of Si-T91 and Si-316SS specimens after corrosion test at 550°C
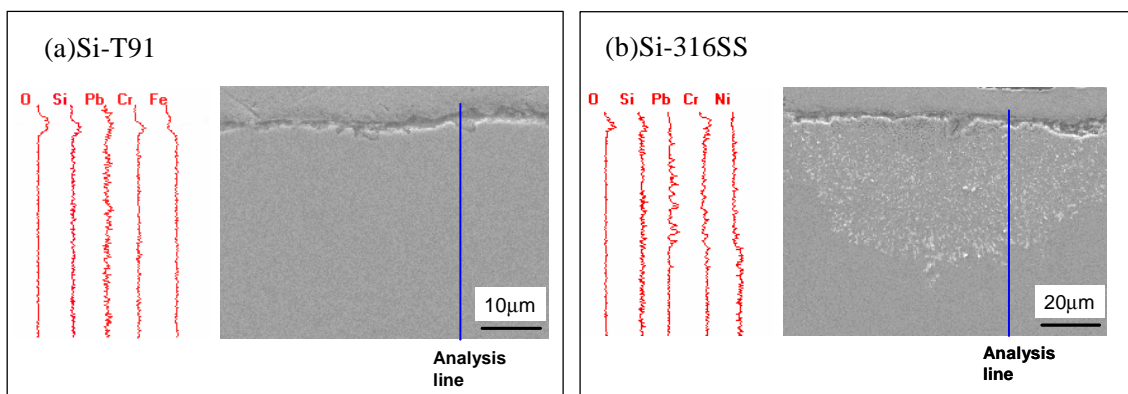
Due to the occurrence of local ferritisation, it was difficult to completely prevent ferritisation in liquid LBE when Si-316SS containing about 2.5% Si and LeCor containing about 5% Si were tested in oxygen-saturated LBE at 550°C. In case of Si-T91, corrosion resistance was improved through formation of the oxide film containing Si and Cr at 550°C under the oxygen-saturated condition. Since the protectiveness of the oxide film may change depending on the environmental condition, it is necessary to study the stability of the oxide film under the low oxygen concentration condition. Furthermore, it is also necessary to investigate irradiation behaviour of Si-enriched steels because it is anticipated that Si in steels, in particular martensitic steels, degrades irradiation properties.

Conclusions

Experimental results obtained from corrosion tests of various steels in liquid LBE at temperatures from 450°C to 600°C are summarised as follows:

- Temperature increase produces active corrosion. Corrosion becomes severe when the temperature exceeds 500°C. Grain boundary corrosion, penetration of LBE and/or ferritisation occur in most steels at 550°C. In particular, such corrosion attack is very violent at 600°C and the corrosion depth of 316SS is above 500 μm for 2 000 h. SX containing 5% Si exhibits good corrosion resistance.

- Oxygen concentration dependence of corrosion is found clearly. Corrosion attack becomes severe in most steels when the oxygen concentration decreases from the oxygen-saturated condition to 10^{-9} wt.% or 10^{-8} wt.%. Although the influence is small in T91 and SX, dissolution occurs in pure iron and ferritisation proceeds in 316SS at 450°C under the low oxygen concentration condition. At 550°C, the corrosion depths of T91, pure iron and 316SS become very large and local ferritisation occurs in SX with the decrease in oxygen concentration.

- Corrosion resistance is improved in Si-T91 containing 1.5% Si and Si-316SS containing about 2.5% Si in oxygen-saturated LBE at 550°C in comparison with that of normal T91 and 316SS. In the case of 316SS, it is difficult to prevent ferritisation completely due to the occurrence of local ferritisation by means of addition of about 2.5% Si to 316SS.

References

[1]   Gorynin, I.V., G.P. Karzov, V.G. Markov, V.S. Lavrukihin, V.A. Yakovlev, *Proceedings of Heavy Liquid Metal Coolants in Nuclear Technology, HLMC'98*, 5-9 October 1998, Obninsk, Russia (1999), p. 120.

[2]   Yachmenyov, G.S., A.Ye. Rusanov, B.F. Gromov, Yu.S. Belomytsev, N.S. Skvortsov, A.P. Demishonkov, *Proceedings of Heavy Liquid Metal Coolants in Nuclear Technology, HLMC'98*, 5-9 October 1998, Obninsk, Russia (1999), p. 133.

[3]   Barbier, F., A. Rusanov, *J. Nucl. Mater.*, 296, 231 (2001).

[4]   Benamati, G., C. Fazio, H. Piankova, A. Rusanov, *J. Nucl. Mater.* 301, 23 (2002).

[5] Nuclear Energy Agency, *Handbook on Lead-bismuth Eutectic Alloy and Lead Properties, Materials Compatibility, Thermal-hydraulics and Technologies*, OECD/NEA, Paris (2007), accessed 29/09/2009 *www.nea.fr/html/science/reports/2007/nea6195-handbook.html*.

[6] Martin, F.J., L. Soler, F. Hernandez, D. Gomez-Briceno, *J. Nucl. Mater.*, 335, 194 (2004).

[7] Kurata, Y., M. Futakawa, S. Saito, *J. Nucl. Mater.*, 343, 333 (2005).

[8] Kurata, Y., M. Futakawa, S. Saito, *J. Nucl. Mater.* 373, 164 (2008).

Flow measurement of high temperature liquid metal using ultrasonic Doppler profiling

Hironari Obayashi
Japan Atomic Energy Agency, Japan

Abstract

Measurement of lead-bismuth eutectic (LBE) flow velocity profile was successfully realised in the spallation target model loop of accelerator-driven system (ADS) by the Ultrasonic Velocity Profiler (UVP) technique. UVP is a powerful tool to measure an instantaneous space-time velocity profile especially on a velocity measurement of an opaque liquid flow, such as liquid metal. However, it has not yet been done well because both of its poor wetting property with stainless steel and of the difficulty in manufacturing probe at high temperature. At lower temperature, wetting of LBE to stainless steel that is a material of target loop is too poor. Therefore, the surface of the test section was treated by polishing, flatting and finally coating with nickel and solder. And we performed velocity measurement along the centreline of the loop and confirmed basic performance of the loop. It was found that there were periodical releases of eddy from the recirculation region formed near the wall surface of the inner cylinder. We made then a measurement for non-parallel directions with the centreline and observed three-dimensional structure of LBE flow configuration. On the other hand, there is not the ultrasonic transducer which can apply to high temperature at more than 300°C. Therefore, the development of the high-temperature transducer that can be used at the high temperature condition is a pressing need because it establishes the velocity measurement techniques for LBE flow. Thus we adopted the acoustic wave guide method and conducted a survey of the suitable guide material for LBE flow by using the wave equation.

Introduction

Liquid metals as a flowing medium

In the industrial processes, metals are treated and processed in liquid state and they are mostly flowing. For instance, in the steel making, a flow of liquid iron plays an important role in determining its operational efficiency of manufacturing processes and also for designing the molten pot and process channels, especially from the thermal insulation point of view. It is also observed for molten metals to play an important role in welding processes. Flow velocity in such situation becomes unexpectedly large due to a high surface tension and low viscosity of liquid metals. On the other hand, in active examples of industrial applications, various liquid metals are used as a flow medium for coolant or reacting materials. Typical one is sodium for fast breeding nuclear reactor (FBR). Other liquid metals are also used in various situations in industry. Among these liquid metals, mercury was convenient since it is in liquid state under room temperature but it is not any more usable due to its toxicity. Sodium is also convenient but as it is reactive with water; its handling requires very careful preventive measures against fire. Gallium is also low melting temperature metal, and it reacts with oxygen in air very radically and a price is too high to use it in a large quantity. Lead-bismuth eutectic (LBE) has advantage to use because its melting temperature is not very high and its chemical state is relatively stable comparative with sodium.

Measurement techniques for liquid metal flow

It is of utmost importance to investigate flow structure and behaviour of liquid metals when it is used in an active manner not only in heat transportation but also a flowing medium, as is the case for any kinds of situations of fluid flow is involved, and as such, fluid mechanics is applied. It is obvious that any optical method of flow measurement such as Particle Image Velocimetry (PIV) and Laser Doppler Velocimetry (LDV) cannot be applied since all the liquid metals are opaque. This meant that non-invasive flow measurement was not possible until the ultrasonic measurement has been established. A single way is to use radiation such as X-ray [1,2] or neutron [3-6] to visualise the flow. However, these methods have no sufficient resolution in space and time for making qualitative evaluation of the flow behaviour. Furthermore, apparatus for them are inconveniently large, expensive and difficult to use so that they were used only under some special conditions and configurations. Hot-wire/film [7] anemometer, thermal sensor [8,9] and magnetic probe [9,10] are all invasive and point wise measurement methods. This is especially disadvantageous for liquid metal flow measurement because high Pr number and low viscosity causes a very different behaviour of momentum and thermal boundary layer around the probe compared with conventional non-metal liquids such a water flow.

### Ultrasonic Velocity Profiling (UVP)

Ultrasonic Velocity Profiler (UVP, see Figure 1) has been established in experimental applications in fluid dynamics and engineering applications involving flow measurements. It is a novel measurement method involving of line measurements and, while measuring a one-dimensional velocity component, it enables obtaining the instantaneous velocity distribution as a function of time, the quantitative spatio-temporal information of the flow field. The use of ultrasonic sound is advantageous in that it makes the method applicable to opaque liquids such as liquid metals and it can be applied non-invasively behind opaque container walls.

Experimental apparatus and configuration for measurement of flowing LBE

JAEA Lead Bismuth Loop-2 (JLBL-2)

JAEA Lead Bismuth Loop-2 (JLBL-2) is a model of the spallation target. It is a closed-loop driven by an electro-magnetic pump. Flow rate of the working fluid driven by this pump is constant and it is observed by an electro-magnetic flow meter. This model loop has coaxially arranged annular and tube channels. The radius of the outer cylinder tube is 63 mm and inner cylinder is 35.5 mm. The gaps between the two coaxial cylinders are 3 mm. And the total length of the loop is 1 504.5 mm. In operating ADS, the temperature of the LBE is expected to reach 500°C. In consideration of the durability and

Figure 1: Schematic illustration of UVP measurement
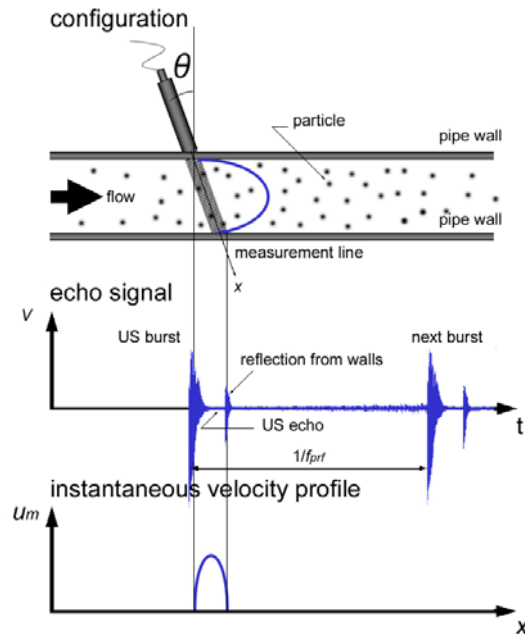
heat-resistant temperatures of high temperature transducers, we set the temperature of LBE to 150°C. Because the surface tension of LBE is very high in the temperature range in the neighbourhood of the melting point, the wetting conditions with the stainless steel pipe wall surface and LBE are very poor. This insufficient wetting condition does not erode the solid surface, but some problems occur in UVP measurement [11].Therefore, the inner surface of the measurement section was treated by polishing, flatting and finally coating with nickel and solder. As a result, wetting condition is improved markedly.

Figure 2: Experimental configuration and illustration of JLBL-2
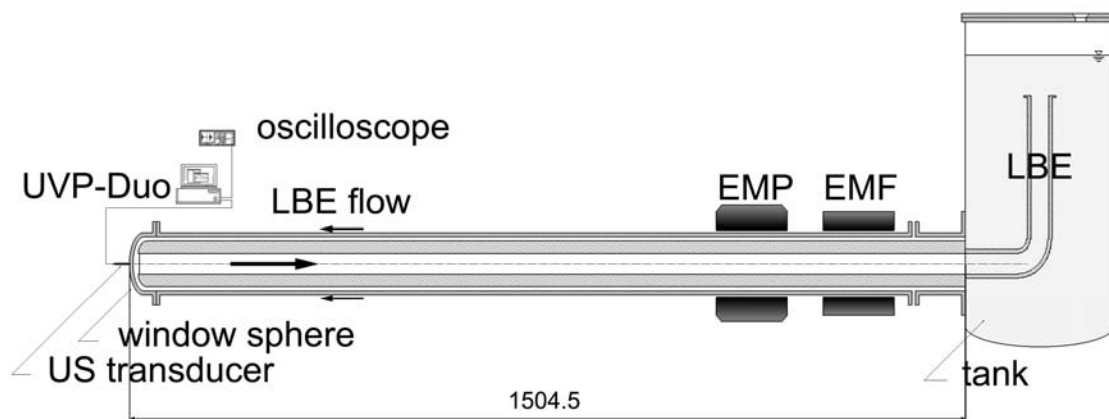
Experimental set-up

The temperature of the loop and the LBE are monitored by a plural thermocouple, and kept uniformly at 150°C. The LBE flow passes the gap between the two cylinders, turns over and then forms the reverse direction flow in the inner cylinder. UVP Monitor model-Duo (Met-Flow) was used for the velocity measurement. A high temperature transducer (Japan probe) undertakes the emission and the reception of the ultrasonic burst signals. We used argon gas bubbles rolled up at the free surface in

the LBE tank as reflectors for the ultrasonic burst signal to be able to trace the LBE flow. The velocity measurement was performed at the edge of the loop end of the window sphere where a proton beam was incident to the target. This window sphere has a spherical shape and is 3.5 mm thick. Figure 3 shows a front view of the measurement window and side view of the test section with measurement line. As shown in the figure, the measurement position is located at the centre of the window sphere, and eight points on an arc have this point as their centre. The radius of this arc is 14 mm, and measurement positions are located at every 45°. As well, the ultrasonic transducer is installed perpendicular to the surface of the window sphere as a countermeasure to prevent the refraction phenomenon of an ultrasonic pulse beam that is caused at the wall surface of the window sphere.

Figure 3: Experimental configuration of the measurement line on the window sphere; window sphere and installing position of an ultrasonic transducer and side view of the test section with measurement line
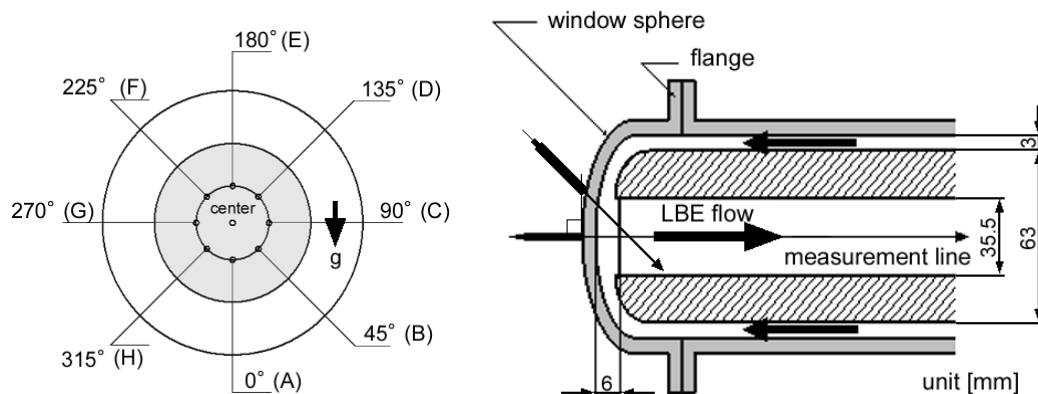

Measurement results

### *Velocity profile along a centreline (JLBL-2)*

We changed the flow rates flowing through the loop and measured the velocity profile at the centreline of the inner cylinder. Experimental results are shown in Figure 4, which presents the velocity profiles of each flow rate at the centreline of the inner cylinder of the loop. In this figure, the horizontal axis represents the measured position and corresponds to the distance on the centreline assuming the edge of the loop as the origin. The vertical axis represents averaged velocity data; that is, the number of averaged velocity profiles is 512. In this experiment, the averaged velocity (U) in the annular region of the loop was changed, and then measured with an electro-magnetic flow meter installed in the upstream side of the loop. The velocity conditions were set to four phases (U = 0.25, 0.50, 0.75 and 1.00 m/s). Under all velocity conditions, in the averaged velocity profiles provided by this experiment the velocity data shows zero data from the starting position of the measurement to a neighbourhood distance of 15 mm. At the inner wall surface of the target window sphere, the LBE flows coming from annular channels collide with each other. Therefore, a local dead region is formed for the LBE flow near the centre of the edge of the loop. It is thought that this result represents a dead region of the LBE flow that extends to the neighbourhood a distance of 15 mm from the inner wall surface at the centre of the loop. Even if the LBE flow rate of in JLBL-2 increases, the formation of this dead region cannot be avoided. When a proton beam is incident in the JLBL-2, countermeasures apart from increasing the LBE flow rate are necessary; further, it is thought that this dead region interferes with the cooling of the target model loop. In the side downstream from the dead region, the velocity profiles are at a maximum in the vicinity of a distance 30 mm, and after having suddenly increased, they gently decrease thereafter. By increasing the velocity conditions, the maximum velocity profiles show a proportional relationship; however, there is no proportional relation in the tendency for a decrease in the velocity after the maximum data is obtained. A recirculation region of the LBE flow is formed on the cylinder pipe wall near the edge of the inner cylinder of the loop. A shrinking flow occurs for the flow in the main direction at any position in this recirculation region. A colour density plot of the data set on the space-time domain, as given in Figure 5. In this figure, velocity condition is

U1. Horizontal axis represents the time, and vertical axis represents the distance on the centreline. Colour represents the velocity. In this figure, almost velocity data is positive. It is observed that there occurs a space-temporal oscillation in the measured area. In this figure, velocity data shows oblique line and appears periodically in time. These lines show the motion of a fluid volume moving on the measurement line. A moving velocity of this volume that calculated by the inclination of the velocity stripes is about 2.3 mm/s. It is thought that this flow structure is eddies that discharged from the recirculation region which moved along the centreline.

Figure 4: Averaged velocity profile at the centreline of JLBL-2, where velocity conditions are U1, U2, U3, U4 = 0.25, 0.50, 0.75, 1.00 m/sec
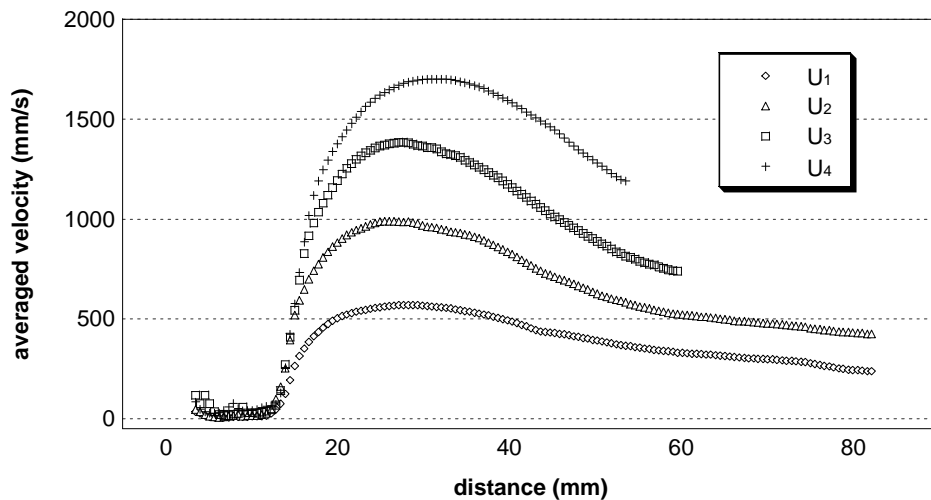
Figure 5: Space-time representation of the time dependent one-dimensional velocity profile, where velocity condition is U$_1$
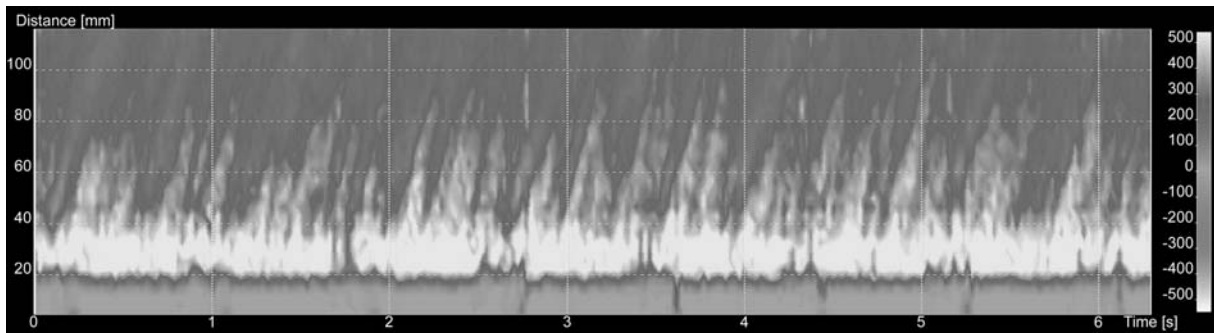

Angular velocity profiles

Figure 6 shows the experimental results of the averaged velocity profiles. Each velocity profile (A) to (H) shows a result measured counter clockwise from positions at intervals of 45°. A velocity condition is U1. This figure represents that the LBE flow is approximately symmetric. In the position near the window sphere, it was observed that the flow of the upper side was fast and the lower side slow. Furthermore, the velocity profiles of the lower side (A, B, H) changes from negative velocity to positive velocity continually. This shows the possibility that an eddy caused by the characteristic of the equipments is formed in the lower side. The size of this eddy depends on the configuration of flow passage.

Figure 6: Averaged velocity profiles measured around the centreline of the measurement window at even intervals of angle, where measurement position labelled with A to G are expressed in Figure 3 and velocity condition is U_1
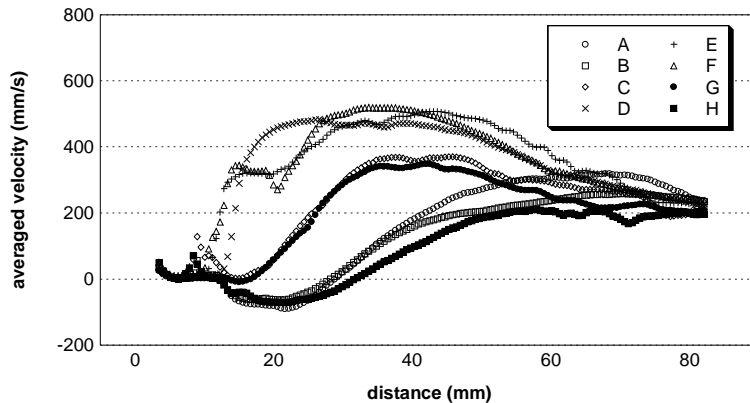
Surveys for high-temperature ultrasonic transducer

Acoustic wave guide transducer

The measurement of LBE flow in JLBL-2 by using UVP, we can obtain following results. In operating ADS, the temperature of the LBE is expected to reach 500°C. Therefore, it is indispensable that the ultrasonic transducer which could apply to a high temperature condition. Lithium niobe oxide ($LiNbO_3$) element and the other piezo elements used for the ultrasonic testing for materials could work at a high temperature condition. $LiNbO_3$ element is used for measurement of sodium flow in fast breeder reactor (FBR); however, the voltage of about 1 000 V is required for operating the transducer because the sensitivity is too bad. In this study, a technique to attach the signal guide to the conventional ultrasonic transducer is developed. This idea was given by S. Eckert and others [14-16]. Their "acoustic wave guide" succeeds in a velocity profile measurement of CuSn flow at 620°C. Therefore, we conducted a survey of the suitable guide material for LBE flow by using the wave equation.

Formation of ultrasonic beam

To estimate the beam formation in LBE and the permeability in guide materials, the sound field was calculated by wave equation:

$$\frac{\partial^2 P(t, x, y)}{\partial t^2} = c(x, y)^2 \left\{ \frac{\partial^2 P(t, x, y)}{\partial x^2} + \frac{\partial^2 P(t, x, y)}{\partial y^2} \right\}$$

A result of wave calculation for a continuous wave signal is shown in Figure 7. The mesh size was 0.02×0.02 mm, and time step was 0.1 nsec. The diameter of was 5 mm, and the frequency of signal was 4 MHz. As for the shape of the guide, the column type was selected. The diameter of the guide was 10 mm, and the length was 30 mm. The material of this guide was SUS304 stainless steel. The target medium was LBE. In this result, it was confirmed that the ultrasonic beam was formed without trouble after the guide material had been penetrated. The comparable result is obtained for other materials.
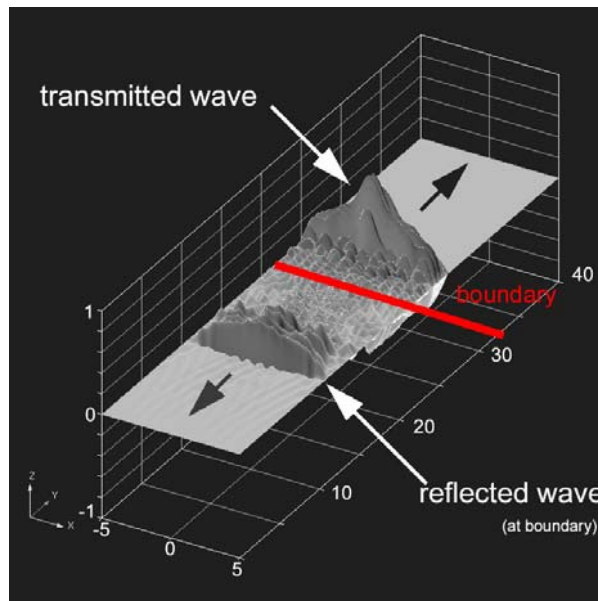
Survey of transmittance for each material

To know the permeability in guide materials, the simulations of wave propagation were conducted by using the pulse signal. The length of guide cylinder was 25 mm. The other parameters were set to the same condition as the previous calculation. The number of cycles was 4. A simulation result is shown in Figure 8. The transmittances for each material obtained by dividing the amplitude of signal that immediately passed through the guide by the amplitude of initial signal were shown in Table 1. In these results, Al and Si showed the good permeability because the acoustic impedance of LBE (Z = 19.6) is a value close to these materials.

**Figure 7: Example of numerical calculation result for confirmation
of beam formation by using continuous signal mode**
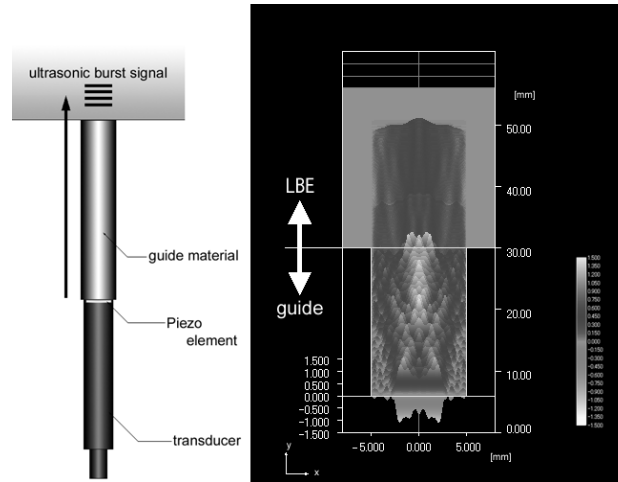
**Figure 8: Example of numerical calculation result for
confirmation of transmittance by using pulse signal mode**

Table 1: Transmittance of pulse signal for each material

Materials	Z [MRayl]	Transmittance [%]
Ti	27.3	35
W	100.9	19
Zr	30.1	33
Mo	63.0	28
SUS304	45.7	30
Al	17.1	48
Si	17.5	52

Summaries

The measurement of LBE flow in JLBL-2 by using UVP, we can obtain the following results:

- There is a space-temporal oscillation that shows the motion of a fluid volume moving on the measurement line near the target window sphere. It is the small eddies that discharged from the recirculation region which moved along and crossed the centreline.

- LBE flow near the target window sphere is approximately symmetric. However, a standing eddy could be formed in the lower side.

- We conducted a survey of the suitable guide material for LBE flow by using the wave equation. As a result, it is forecast that Al and Si are excellent materials.

References

[1] Sherif, H., Abdulla, L. Xin, H. Mark, Anderson, B. Riccardo, L. Michael, Corradini, C. Dae, "Liquid-metal/Water Direct Contact Heat Exchange: Flow Visualization, Flow Stability, and Heat Transfer Using Real-time X-ray Imaging", *Nucl. Sci. Eng.*, Vol. 150-2, 182-220 (2005).

[2] Wildenschild, D., J.W. Hopmans, M.L. Rivers, A.J.R. Kent, "Quantitative Analysis of Flow Processes in a Sand Using Synchrotron-based X-ray Microtomography", *Vadose Zone Journal*, 4, 112-126 (2005).

[3] Sito, *et al.*, "Visualization and Measurements of Liquid Phase Velocity and Void Fraction of Gas-liquid Metal Two-phase Flow by Using Neutron Radiography", *Proc. 9th International Symposium on Flow Visualization* (2000).

[4] Takenaka, N., *et al.*, "Visualization of Streak Lines in Liquid Metal by Neutron Radiography", *Neutron Radiography*, Vol. 4, Gordon and Breach, 355-362 (1993).

[5] Takenaka, N., *et al.*, "Liquid Metal Flow Measurement by Neutron Radiography", *Nucl. Instrum. Methods. Phys. Res. A.*, Vol. 377, 156-160 (1996).

[6] Umekawa, H., *et al.*, "Visualization of Bed Material Movement in a Simulated Fluidized Bed Heat Exchange by Neutron Radiography", *Nucl. Instrum. Methods. Phys. Res. A.*, Vol. 424, 77-83 (1999).

[7] Sadjben, M., "Hot-wire Anemometry in Liquid Mercury", *Rev. Sci. Instrum.*, 36, 945-953 (1965).

[8] Ji, H., W. Fox, D. Pace, "Study of Small Amplitude Magneto Hydrodynamic Surface Waves on Liquid Metal", *Phys. Plasmas*, 012102_1-13 (2005).

[9] Cramer, A., S. Eckert, V. Galindo, G. Gerbeth, B. Willers, W. Witke, "Liquid Metal Model Experiments on Casting and Solidification Processes", *J. Materials Sci.* 39, 7285-7294 (2004).

[10] Men, S., C. Resagk, M. Ziolkowski, M. Kuilekov, H. Brauer, "Measurement of Magnetic Flux Density on a Rotating Distorted Electrolyte-metal Interface", *Meas. Sci. Technol.*, 15, 1323-1326 (2004).

[11] Obayashi, H., Y. Tasaka, M. Morinaga, Y. Takeda, K. Kikuchi, "Measurement of Liquid Metal Flow Using Ultrasonic Velocity Profiler (First Report, Flow Measurement of LBE Target)", *Journal of JSME*, 72, 642-628 (2006).

[12] Takeda, Y., "Measurement of Velocity Profile of Mercury Flow by Ultrasound Doppler Shift Method", *Nucl. Tech.*, Vol. 79, 120-124 (1987).

[13] Kikura, H., Y. Takeda, "Flow Mapping Using Ultrasonic Doppler Method", *ASME Fluid Eng. Division Summer Meeting,* FED-Vol. 245 FEDSM98-5084 (1987).

[14]   Eckert, S., *et al.*, "Velocity Measurement at High Temperatures by Ultrasound Doppler Velocimetry Using an Acoustic Wave Guide", *Exp. in Fluids*, 35, 381-388 (2003).

[15]   Cramer, A., *et al.*, Liquid Metal Model Experiments on Casting and Solidification Processes", *J. Materials Sci.*, 39, 7285-7294 (2004).

[16]   Eckert, S., *et al.*, "Velocity Measurements in Metallic Melts", *Proc. FEDSM2005-77089* (2005).